The Magnetization of an Underwater Caldera: A Time-Lapse Magnetic Anomaly Study of Axial Seamount Bailey Fluegel<sup>1,2</sup>, Maurice Tivey<sup>1\*</sup>, Joseph Biasi<sup>3,4</sup>, William W. Chadwick Jr. <sup>5</sup>, and Scott L. Nooner<sup>6</sup> <sup>1</sup>Woods Hole Oceanographic Institution, Woods Hole, MA <sup>2</sup>Northwestern University, Evanston, IL <sup>3</sup>Dartmouth College, NH <sup>4</sup>University of Oregon, OR <sup>5</sup>Oregon State University, OR <sup>6</sup>University North Carolina Wilmington, NC \*corresponding author Corresponding author: Maurice Tivey (mtivey@whoi.edu) **Keywords:** Magnetism, seamounts, volcanic hazards, volcanology, monitoring 

#### **Key Points:**

- Repeat magnetic surveys at active submarine volcanos image temporal change in thermal structure related to geologic and volcanic processes
  - High resolution magnetic data can be used for low-cost volcano monitoring in the marine environment over relevant timescales

33 Abstract

Axial Seamount in the northeast Pacific erupted in 2015, 2011, and 1998. Although monitored by the Regional Cabled Array of the Ocean Observatory Initiative, few magnetic surveys have been conducted over the region. This study uses high-resolution magnetic data over the seamount collected by autonomous underwater vehicle *Sentry* during three years (2015, 2017, 2020). The goal is to investigate whether there are temporal changes in the near-surface magnetic field observable over the time scale of one volcanic cycle. We compare magnetic maps from repeated tracklines from each year. We find maps of the yearly difference in magnetization show coherent patterns that are not random. The central region of the caldera has become more magnetic during recent years, suggesting cooling of the surficial lava flows since 2015. *Sentry* data are more sensitive to shallow crustal structure compared to sea surface data which show longer wavelength anomalies extending deeper into the crust.

## **Plain Language Summary**

Axial Seamount is an active underwater volcano located off the coast of Oregon that has recently erupted in 2015, 2011, and 1998. Though Axial is monitored by many seafloor instruments, the magnetism of the region and how it changes with time has not been studied. However, we believe studying the magnetics of Axial can provide powerful insights into the internal structure of the volcano. Specifically, volcanic rocks contain magnetic minerals called magnetite. Above a certain temperature, called the Curie temperature, these minerals become non-magnetic. Thus, magnetism may be able to detect changes in the high temperature areas of the volcano between eruptions, such as the magma chamber or young lava flows. Here, we perform the first study analyzing three separate years of high-resolution magnetic data collected using an autonomous underwater vehicle over Axial seamount. We create magnetic maps using repeated vehicle tracklines to highlight differences between each year and compare our findings with broader surveys of the region. Our results indicate the central region of Axial has become more magnetic during recent years, suggesting cooling of the lavas erupted in 2015 and their associated subsurface feeder zones.

### 1 Introduction

Axial Seamount is the most active underwater volcano in the northeast Pacific located ~480 km off the coast of Oregon (45°56′N, 130°00′W). It is situated on the diverging midocean ridge boundary of the Juan de Fuca and Pacific plates, which has an intermediate spreading rate of 5-6 cm/yr (Wilson, 1988; Fig. 1). It is also the location of the world's first underwater volcano observatory NeMO (New Millennium Observatory) and since 2014 has been the location of the National Science Foundation's Ocean Observatory Initiative (OOI) Regional Cabled Array (RCA), which records real-time data from a network of monitoring instruments (Kelley et al., 2014; Embley and Baker, 1999). The volcano rises to a depth of about 1,400 m and has a distinct 3 x 8 km horseshoe-shaped caldera present at its summit (Fig. 1). The caldera walls rise about 100 m above the caldera floor. The caldera floor is comprised of unsedimented basaltic lava flows and active hydrothermal vent systems are found along the caldera margin faults.

Axial Seamount is very active and erupted most recently in 2015, as well as in 2011 and 1998 (Caress et al., 2012; Chadwick et al., 2013, 2016). Based on current inflation rates of the area measured geodetically, it is forecast to erupt again between 2025-2030 but is being continuously monitored in order to adjust this forecast window as rates change (https://www.pmel.noaa.gov/eoi/axial\_blog.html). Since the 2015 eruption, Axial has re-inflated to ~90% of its pre-eruption level and the continuous inflation since the last eruption implies ongoing replenishment of the magma reservoir (Chadwick et al., 2022), which could cause a noticeable warming of the subcrustal region beneath the seamount. However, the rate of inflation has noticeably slowed in recent years prompting a widening of the eruption forecast window (Chadwick et al., 2022).

Axial has been the focus of many geophysical studies due to its frequent activity, including geodetic, seismic, and gravity surveys (e.g. Arnulf et al., 2014; 2018; Caratori-Tontini et al., 2016; Carbotte et al., 2020; Hefner et al., 2020; Hildebrand et al., 1990; Nooner and Chadwick, 2009; 2016; Waldhauser et al., 2020; West et al., 2001; 2003; Wilcock et al., 2016; 2018). However, to date, few magnetic studies have been undertaken over the region. In 1990, sea surface magnetic data were compiled from several cruises to investigate the magnetic structure of the seamount (Tivey and Johnson, 1990). Tivey and Johnson (1990) discovered negative anomalies at the summit, and through modeling, determined that the anomalies could be

explained by a drastically thinned (<700 m) magnetic source layer. The conclusion was that Axial displayed the thermal effects of a shallow magma chamber. More recent seismic imaging of Axial confirms the presence of an elongate magma chamber (MMR in Fig. 1) beneath the summit caldera of Axial (Arnulf et al., 2014; 2018; Carbotte et al., 2020) and a smaller secondary reservoir to the east (SMR in Fig. 1). The thermal signature of the main magma chamber, the internal lava feeder system, and the slow re-inflation of the summit since 2015 may be detectable using magnetic fields (Biasi et al., this issue). Here, we present the first study of temporal magnetic imaging using repeat surveys of high-resolution, near-bottom magnetic data gathered over the summit of Axial Seamount since 2015 with the autonomous underwater vehicle (AUV) *Sentry*. The aim of this study is to determine if there are observable temporal changes in the magnetic signature of Axial following the last eruption, and what such variations imply about the internal structure of the volcano.

The basaltic volcanic rocks of Axial Seamount, which contain magnetite, become nonmagnetic above the Curie temperature of magnetite of 580°C. Alteration and titanium substitution within magnetite can lower the Curie temperature (Dunlop & Ozdemir, 1997) to between 150° and 400°C (Gee and Kent, 2007). We note that this study investigates the difference in magnetism and while we don't know the absolute Curie temperature of the crust, it is unlikely to have changed significantly due to alteration over such a short 5-year period. Therefore, regions of high temperature above the Curie temperature surrounding and including the magma chamber should appear as non-magnetic anomalies within the data. This thermally demagnetized zone may grow prior to an impending eruption due to the inflation of the magma chamber that is known to occur prior to eruptions (Chadwick et al., 2022; Nooner and Chadwick, 2016). If true, we may be able to measure magnetic changes in this zone as it enlarges (Biasi et al., this issue). However, it is also possible that seawater circulation within the shallow fractured crust overlying the magma chamber would keep the crust cool creating a cold lid that would restrict the extent of the thermal zone to some depth and may only change once lava has erupted to the surface. In this case, immediately following an eruption we may see a cooling and an increase in magnetism locally. Our data analysis may help determine which of these thermal zone hypotheses is supported by evidence. Furthermore, if successful, magnetic surveys may provide a low-cost and efficient method for gathering frequent temporal data in comparison to

other forms of geophysical surveys (Biasi et al., this issue), and could provide valuable insights into the internal workings of Axial Seamount.

#### 2 Methods

Several recent expeditions have collected repeated bathymetric lines at Axial Seamount for geodetic purposes using the AUV *Sentry* operated by the National Deep Submergence Facility (NDSF) at Woods Hole Oceanographic Institution (WHOI) (Caress et al., 2020; Hefner et al., 2021). Three separate Applied Physics Systems model-1540 3-axis digital vector magnetometers are mounted on *Sentry* with one on top, and one on each of the starboard and port sides of the vehicle. The housings are made of non-magnetic titanium and collect continuous three-component magnetic field measurements. Data gathered from the top magnetometer are used for interpretation as the other two are heavily affected by the internal equipment of the vehicle as it moves. During the repeat bathymetric surveys in 2015, 2017, and 2020 (during cruises TN327, RR1712, and TN383), *Sentry* typically flew at an altitude of ~65 m above the bottom and collected magnetic field data along the tracklines covering much of the summit region (Fig. 2).

The magnetometer sensors used on *Sentry* are not absolute field measuring devices. Therefore, the data must be calibrated to remove the permanent and induced effects of the vehicle on the magnetic field response. *Sentry* is programmed to carry out calibration spins at the beginning or end of each dive. Three magnetic field components (X, Y, and Z) are recorded. During the calibration turns, the vehicle spins and although individual components change, the total magnetic field (vector sum of the components) should not change since *Sentry* remains in essentially one location. By examining the total magnetic field during the calibration spins, any field offsets resulting from the local field of the vehicle or any induced field effects can be measured. If any offsets are detected, they are corrected for prior to processing.

We used two primary methods of calibration: full-vector calibration and compass-swing (Tivey et al., 2014; Xu and Tivey, 2016). The compass-swing method first corrects for the local field effect of the vehicle, and then corrects for the induced field effects assuming the vehicle is only spinning in the horizontal plane. This results in a calibrated total magnetic field (See

supplemental material, Fig. S1). However, the compass-swing method does not account for the magnetic effects of pitch and roll changes of the vehicle (though these typically are not significant) and is used in situations where attitude information is lacking. We can only use the vector summed total field from this calibration. For this project, compass-swing calibration was used for the 2015 and 2017 dive data. The full-vector calibration technique (Tivey et al., 2014) involves using measured attitude data to correct for the full effects of the vehicle motion on the magnetic measurements and results in all three components being corrected and usable. This method was used for the 2020 dive data as full attitude information was provided with this data set, unlike those for 2015 and 2017 (See supplemental material, Fig. S2). Detrending is used for both methods if a long-term trend is present. Generally during a calibration spin, the permanent magnetic field effect of Sentry is on the order of 500 nT and the International Geomagnetic Reference Field (IGRF) model allows us to estimate total field intensity for the date and location of the survey to successfully correct the data. These calibration methods were performed separately on all dives for each survey year (six dives in 2015, five dives in 2017, and seven dives in 2020). We obtained error bars typically less than 100 nT (with an average of  $59 \pm 24$  nT between all the dives) for the local and induced field effects (Table-1 Supplementary material), allowing us to have great confidence in our results, since magnetic field anomalies over Axial caldera are typically a few thousand nanotesla.

After calibration, the data are ready to be processed. The first step of processing involved interpolation onto a grid by resampling to equally spaced points to ensure comparable resolution between different surveys as well as to allow for further processing. To create grids for each year, tracklines were matched to include only those that were repeated between each of the three years to ensure the resolution between the yearly maps was the same (Fig. 2 g,h,i). We used a continuous minimum curvature algorithm for the gridding at a node spacing of 0.25 min/~460 m (Wessel and Smith, 1991).

After the data were interpolated onto grids they were upward continued to a level, horizontal plane above the topography (at 1.4 km depth). This was done using an iterative Fast Fourier Transform method to reduce magnetic measurements made on an uneven plane which is necessary to minimize the effects of topography as well as prepare the data for further transformations such as reduction to the pole or frequency-domain inversion (Guspi, 1987). In

order to minimize edge effects, the *Sentry* data grids were embedded within a broader regional grid of magnetic anomalies downward continued from the sea surface. The resultant *Sentry* upward continued field grids (Fig. 2a,b,c) were then used along with bathymetry to invert for crustal magnetization (Fig. 2d,e,f) for a source layer of constant thickness of 1 km and a time-averaged direction of magnetization based on the Geocentric Axial Dipole hypothesis (Inclination 66° and Declination 0°). We used a Fast Fourier Transform technique, which removes the topographic effect from the magnetic field to determine source magnetization (Parker and Huestis, 1974). A nominal constant thickness of 1 km was used in the absence of any detailed knowledge about the thickness of the source layer, although seismic data indicates a volcanic lid of 1+ km thickness above the magma chamber (Arnulf et al. 2014; 2018). We note that considering the altitude of the survey above the seafloor of less than 100 m the inversion result is more sensitive to shallow structure than the overall layer thickness.

Given that Axial is a young feature it should be of normal polarity (i.e. northward directed magnetization within the present-day normal polarity Brunhes chron). The magnetization inversion solution is always zero-meaned and so shows both apparent normal and reversed polarities. To correct for this we compute an annihilator, which is a magnetization which when convolved with bathymetry produces a zero magnetic field (see Parker and Huestis, 1974 for details of annihilator computation). We then add the annihilator multiplied by a scalar value to the inversion such that the zero level is adjusted so that the magnetization is all normal (i.e. positive) polarity. Typically, this has little effect on the relative shape and magnitude of the calculated anomalies. For all of the maps we added 10 times the annihilator to the inversion solutions. Once this final step is complete, the data are ready for interpretation.

#### 3 Results and Discussion

To provide greater regional context for the *Sentry* magnetic field data, we first combined sea surface data from a recent R/V Langseth ship-based survey in 2019 (MGL2019) with other existing ship magnetic data coverage from the Marine Geoscience Data System (MGDS). Since the data are gathered over a larger region that is further away from the seafloor than the near bottom data (and ~2.5 km away from the magma chamber), the ship data are therefore capable of imaging longer wavelength signals that originate deeper beneath the seafloor. The gridded and

reduced-to-the-pole sea surface anomaly (Fig. 3) shows a narrow magnetic anomaly low crossing the summit caldera region as previously reported in the 1990 study (Tivey and Johnson, 1990). Magnetic highs extend northwards along the North Rift Zone and south along the upper South Rift Zone. The western Brunhes-Matuyama reversal boundary is located just north and west of the seamount (Fig. 3). The low magnetic anomaly over the caldera aligns with the seismically detected main magma chamber (MMR) but the secondary SMR region does not have a similar magnetic low (Fig. 3). Unfortunately, there is not sufficient sea surface coverage collected on a temporal basis to resolve any changes with time and so we can only resolve the static magnetic contrasts with these data.

211

212

213

214

215

216

217

218

219

220

221

222

223

224

225

226

227

228

229

230

231

232

233

234

235

236

237

238

239

240

241

The repeated *Sentry* surveys for each year are able to resolve shorter wavelength features which reflect variations of the shallower crustal layers of the summit magnetism (see Sentry tracklines of Fig. 2g,h,i). The upward continued Sentry magnetic field maps (at the 1.4 km depth level) show a broad anomaly low over the caldera but with shorter wavelength anomalies within the caldera (Fig. 2a,b,c). Magnetic highs can be seen to the north and south of caldera along the rift zones, as in the ship-based results. The amplitude of the anomalies is on the order of a few thousand nanotesla, meaning the anomalies we see are significant as they are well beyond the uncertainties of sensor calibration. Inversion results, adjusted by the annihilator, indicate magnetization values ranging from 0-30 A/m. The magnetization maps also show variability over the caldera region from year to year (Fig. 2 d,e,f). Specifically, it appears the northern caldera region has become more magnetic over time, possibly indicating that it has cooled down so that more of the crust has become magnetic. The magnetization maps are based on a 1 km thick layer so any increase in magnetization likely indicates thickening of the magnetized source region (i.e. an increase in the volume of magnetized rock) rather than an increase in magnetization intensity of the rocks themselves. While secondary magnetization as a result of alteration is possible, given the short 5-year timeframe of the study, it is unlikely that alteration processes could rapidly change magnetization on this timescale. Differences between the 2015 to 2017, 2017 to 2020, and 2015 to 2020 magnetic maps show that this variation appears to be consistent over time, becoming more magnetic as time progresses (Fig. 4). There is a large almost 8 A/m increase in magnetization between 2015 and 2017 and then relatively little increase after that between 2017 and 2020 (Fig. 4). This change seems to be limited to within the caldera region, indicating that the signal is spatially coherent and not random. The volcano last erupted

in 2015 with thin (<10 m) lava flows in the NE part of the caldera and on the NE rim, and thicker flows (>100 m) further north on the rift zone (Chadwick et al., 2016; Clague et al., 2017). Therefore, we interpret these anomalies between successive years as being a cooling and magnetizing effect of the emplacement of the 2015 lava sequences. We suggest that the lava flows and internal lava feeder system of the eruption may have still been warm when *Sentry* surveyed the region in 2015 only four months after the eruption, but since then the lavas flows and underlying crust have cooled and become magnetized, consequently causing the observed increase in magnetism over the following two years. This is consistent with independent geophysical data (Chadwick et al., 2022) which shows that Axial, while it has inflated to ~90% of its pre-eruption level, has a magma supply rate that has been waning since the last eruption in 2015, so that any future eruption is still years away. Furthermore, magnetic modeling of Axial Seamount (Biasi et al., this issue) shows that while a thermal zone extends beyond the magma body itself, the northern part of the caldera needed extensive cooling to replicate the results reported here.

The *Sentry* results show that these high-resolution near-bottom magnetic grids are more sensitive to shallow crustal features, primarily because of the limited spatial extent of the surveys limiting long-wavelength sensitivity but with an ability to sample shorter wavelengths. In contrast, the sea surface surveys, or at least those of broader regional coverage, are able to detect longer wavelength signals coming from deeper structures, such as the magma chamber thermal zone located 1-2 km below the ocean floor. The sea surface results (Fig. 3) show the narrow magnetic anomaly low over the summit caldera region (Tivey and Johnson, 1990) aligned with the seismic imaging of the sub-caldera magma chamber (Arnulf et al., 2014; 2018).

#### 4. Conclusions

We examined the magnetic field differences between AUV surveys at Axial Seamount in 2015, 2017 and 2020, and conclude that the magnetic patterns are coherent and not random relative to caldera structure, and that the differences in magnetic field are above the noise level of the calibrations. The results indicate that seafloor magnetic field measurements from near-bottom AUV surveys can be used to image temporal changes in shallow thermal structure and that the anomalies relate to geologic structure. Specifically, we found that the central region of

the caldera appears to be getting more magnetic over the past few years following the eruption in 2015, apparently related to the cooling of surficial lava flows. On the other hand, we note that more regional ship-based results show longer wavelength anomalies that reflect deeper structure within Axial Seamount, such as a low magnetization zone surrounding the sub-caldera magma reservoir.

These results show that magnetic surveys can yield valuable information about crustal structure on several spatial scales related to magmatic activity and should be considered for future expeditions at active submarine volcanoes such as Axial Seamount, especially since they can be piggybacked on other surveys, as in this study. It remains to be tested whether near bottom magnetic field surveys that are spatially broader in scope could detect longer wavelength magnetic anomalies related to the sub-caldera magma chamber thermal region. In the future, we hope to examine whether such variations may be detectable in other ways, such as by wider range AUV surveys or repeated ship-based magnetic surveys, and believe that more magnetic surveys should be completed at Axial in upcoming years to search for other insightful temporal changes.

## Acknowledgements

Fluegel was supported by a Woods Hole Oceanographic Institution Summer Student Fellowship in 2021. Tivey was supported under a Woods Hole Oceanographic Institution independent research grant. Biasi was supported by NSF grant 2052963. Sentry data collection by Chadwick and Nooner was supported by NSF grants 1356839 and 1736882. We thank Sean Kelley and the AUV *Sentry* operations teams for the data collection over the many campaigns at Axial Seamount. The authors are not aware of any conflicts of interest that would affect this manuscript.

# **Credit Authorship Statement**

B. Fluegel – Data analysis, Methodology, Visualization, Writing – original draft, Writing review and editing. M. Tivey – Conceptualization, Data curation, Funding Acquisition, Methodology, Project administration, Resources, Supervision, Validation, Visualization, Writing

- original draft, Writing - review and editing. J. Biasi - Conceptualization, Writing - review and 301 editing. W. Chadwick – Data collection, Funding Data Acquisition, Writing – review and 302 editing. S. Nooner – Data collection, Funding Data Acquisition, Writing – review and editing. 303 304 **Open Research** 305 The Sentry magnetic data used in the study are available at the Marine Geoscience Data 306 System (MGDS) located at Lamont Doherty Earth Observatory via https://www.marine-geo.org. 307 The 2020 Sentry data are available at <a href="https://www.marine-">https://www.marine-</a> 308 geo.org/tools/search/Files.php?data\_set\_uid=30204 (MGDS DOI: 10.26022/IEDA/330204\_ref: 309 Chadwick, W.; Nooner, S. and D. Caress, 2021, AUV Sentry dive navigation and along-track 310 data at Axial Seamount (TN383, 2020). IEDA). The 2015 Cruise TN327 (DOI: 10.7284/901818) 311 Sentry data (doi:10.26022/IEDA/331045) are available at MGDS: https://www.marine-312 geo.org/tools/files/31045. The 2017 Cruise (RR1712 DOI: 10.7284/907493) Sentry data 313 (doi:10.26022/IEDA331046) are available at: https://www.marine-geo.org/tools/files/31046. 314 315 The sea surface magnetic data from CRUISE MGL1905 can be found at https://www.rvdata.us/search/cruise/MGL1905 and MGDS and older magnetic data is from the 316

MGDS portal over the Axial Seamount region.

317

## 319 References

- Arnulf, A. F., Harding, A. J., Kent, G. M., Carbotte, S. M., Canales, J. P., & Nedimovic, M. R.
- 321 (2014). Anatomy of an active submarine volcano. *Geology*, 42(8), 655-658.
- 322 https://doi.org/10.1130/G35629.1
- Arnulf, A. F., Harding, A. J., Kent, G. M., & Wilcock, W. S. D. (2018). Structure, seismicity,
- and accretionary processes at the hot spot-influenced Axial Seamount on the Juan de
- Fuca Ridge. *Journal of Geophysical Research: Solid Earth*, 123, 4618–4646.
- Biasi, J., M. Tivey, & B. Fluegel, (this issue). Volcano Monitoring with Magnetic
- Measurements: A Simulation of Eruptions at Axial Seamount, Kilauea, Bárðarbunga, and
- Mount Saint Helens, Geophysical Research Letters, [companion paper also in review at
- 329 GRL].
- Caratori Tontini, F., T. Crone, C.E.J. de Ronde, D.J. Fornari, J. Kinsey, E. Mittelstaedt, and M.
- Tivey, Crustal magnetization and the subseafloor structure of the ASHES vent field
- (Axial Seamount, Juan de Fuca Ridge): Implications for the exploration of hydrothermal
- sites, Geophys. Res. Lett., 43, doi: 10.1002/2016GL069430, 2016.
- Carbotte, S. M., Arnulf, A. F., Spiegelman, M., Lee, M., Harding, A., Kent, G., Canales, J. P., &
- Nedimovic, M. (2020). Stacked sills forming a deep melt-mush feeder conduit beneath
- Axial Seamount. *Geology*, 48, 693–697. https://doi.org/10.1130/G47223.1
- Caress, D. W., Clague, D. A., Paduan, J. B., Chadwick, W. W., Jr., Nooner, S. L., & Thomas, H.
- J. (2020). Vertical Deformation of the Axial Seamount Summit from Repeated 1-m Scale
- Bathymetry Surveys Using AUVs. Abstract V040-0017 presented at 2020 Fall Meeting,
- 340 AGU, San Francisco, CA, 7-11 Dec.
- Caress, D. W., Clague, D. A., Paduan, J. B., Martin, J., Dreyer, B., Chadwick, W. W., Jr., Denny,
- A., & Kelley, D. S. (2012). Repeat bathymetric surveys at 1-metre resolution of lava
- flows erupted at Axial Seamount in April 2011. *Nature Geosci.*, 5(7), 483-488.
- 344 https://doi.org/10.1038/NGEO1496
- Chadwick, W. W., Jr, Clague, D. A., Embley, R. W., Perfit, M. R., Butterfield, D. A., Caress,
- 346 D.W., Paduan, J. B., Martin, J. F., Sasnett, P., Merle, S. G., & Bobbitt, A. M. (2013). The

- 1998 eruption of Axial Seamount: New insights on submarine lava flow emplacement
- from high-resolution mapping. *Geochemistry Geophysics Geosystems*, 14, 3939–3968.
- 349 https://doi.org/10.1002/ggge.20202
- Chadwick, W. W., Jr, Paduan, J. B., Clague, D. A., Dreyer, B. M., Merle, S. G., Bobbitt, A. M.,
- Caress, D. W., Philip, B. T., Kelley, D. S., & Nooner, S. L. (2016). Voluminous eruption
- from a zoned magma body after an increase in supply rate at Axial Seamount, *Geophys*.
- 353 Res. Lett., 43, 12,063–12,070. https://doi.org/10.1002/2016GL071327
- Chadwick, W. W., Jr., Wilcock, W. S. D., Nooner, S. L., Beeson, J. W., Sawyer, A. M., & Lau
- T. K. (2022). Geodetic Monitoring at Axial Seamount Since its 2015 Eruption Reveals a
- Waning Magma Supply and Tightly Linked Rates of Deformation and Seismicity.
- *Geochemistry Geophysics Geosystems*, 22. https://doi.org/10.1029/2021GC010153.
- Clague, D. A., Paduan, J. B., Caress, D. W., Chadwick, W. W., Jr., Saout, M. L., Dreyer, B., &
- Portner, R. (2017). High-resolution AUV mapping and targeted ROV observations of
- three historical lava flows at Axial Seamount. *Oceanography*, 30(4), 82-99.
- 361 https://doi.org/10.5670/oceanog.2017.426
- Dunlop, D., & Özdemir, Ö. (1997). Rock Magnetism: Fundamentals and Frontiers (Cambridge
- 363 Studies in Magnetism). Cambridge: Cambridge University Press.
- 364 https://doi.org/10.1017/CBO9780511612794
- Embley, R. W., & Baker, E. T. (1999). Interdisciplinary group explores seafloor eruption with
- remotely operated vehicle. *Eos Trans. AGU*, 80(19), 213.
- Gee, J. S., & Kent, D. V. (2007). Source of oceanic magnetic anomalies and the geomagnetic
- polarity time scale, Treatise on Geophysics, 5, p. 455-507.
- Guspi, F. (1987). Frequency-domain reduction of potential field measurements to a horizontal
- plane. Geoexploration, 24, 87-98.
- Hefner, W., Nooner, S. L., Chadwick, W. W., Jr., & Bohnenstiehl, D. W. R. (2020). Revised
- magmatic source models for the 2015 eruption at Axial Seamount including estimates of
- fault-induced deformation. *Journal of Geophysical Research: Solid Earth*, 125(4).
- 374 https://doi.org/10.1029/2020JB019356

- Hefner, W. L., Nooner, S. L., Chadwick, W. W., Jr., Caress, D. W., Paduan, J. B., Bohnenstiehl,
- D. R., & Clague, D. A. (2021). Deformation Models for the 2015-Eruption and Post-
- Eruption Inflation at Axial Seamount from Repeat AUV Bathymetry. Abstract V45B-
- 378 0138 presented at 2021 Fall Meeting, AGU, New Orleans, LA, 13-17 Dec.
- Hildebrand, J. A., Stevenson, J. M., Hammer, P. T. C., Zumberge, M. A., Parker, R. L., Fox, C.
- G., & Meis, P. J. (1990). A sea floor and sea surface gravity survey of Axial Volcano. J.
- 381 *Geophys. Res.*, 95, 12751-12763.
- Kelley, D. S., Delaney, J. R., & Juniper, S. K. (2014). Establishing a new era of submarine
- volcanic observatories: Cabling Axial Seamount and the Endeavour Segment of the Juan
- de Fuca Ridge. *Mar. Geol.*, 352, 426-450. https://doi.org/10.1016/j.margeo.2014.03.010
- Nooner, S. L., & Chadwick, W. W., Jr. (2009). Volcanic inflation measured in the caldera of
- Axial Seamount: Implications for magma supply and future eruptions. *Geochemistry*,
- 387 Geophysics, Geosystems, 10, Q02002.
- Nooner, S. L., and Chadwick, W. W., Jr. (2016). Inflation-predictable behavior and co-eruption
- deformation at Axial Seamount. *Science*, 354, 1399–1403.
- 390 https://doi.org/10.1126/science.aah4666
- Parker, R. L., & Huestis, S. P. (1974). The inversion of magnetic anomalies in the presence of
- topography. *Journal of Geophysical Research*, 79, 1587-1594.
- Tivey, M., & Johnson, H. (1990). The magnetic structure of Axial Seamount, Juan de Fuca
- Ridge. Journal of Geophysical Research, 95, 12735-12750.
- Tivey, M.A., H.P. Johnson, M.S. Salmi, and M. Hutnak (2014). High-resolution near-bottom
- vector magnetic anomalies over Raven Hydrothermal Field, Endeavour Segment, Juan de
- Fuca Ridge, J. Geophys. Res., 119, doi:10.1002/2014JB011223.
- Waldhauser, F., Wilcock, W. S. D., Tolstoy, M., Baillard, C., Tan Y. J., & Schaff, D. P. (2020).
- Precision seismic monitoring and analysis at Axial Seamount using a real-time doubled-
- 400 difference system. *Journal of Geophysical Research*: Solid Earth, 125.
- Wessel, P., & Smith, W. H. F. (1991). Free software helps map and display data, EOS Trans.
- 402 AGU, 72, 441.

403	West, M., Menke, W., & Tolstoy, M., (2003). Focused magma supply at the intersection of the
404	Cobb hotspot and the Juan de Fuca Ridge. Geophysical Research Letters, 30, 1724.
405	https://doi.org/10.1029/2003GL017104
406	West, M. E., Menke, W., Tolstoy, M., Webb, S., & Sohn, R. (2001). Magma storage beneath
407	Axial Volcano on the Juan de Fuca mid-ocean ridge. Nature, 413, 833-836.
408	Wilcock, W. S. D., Dziak, R. P., Tolstoy, M., Chadwick, W. W., Jr., Nooner, S. L.,
409	Bohnenstiehl, D. R., Caplan-Auerbach, J., Waldhauser, F., Arnulf, A. F., Baillard, C.,
410	Lau, T. K., Haxel, J. H., Tan, Y. J., Garcia, C., Levy, S., & Mann, M. E. (2018). The
411	recent volcanic history of Axial Seamount: Geophysical insights into past eruption
412	dynamics with an eye toward enhanced observations of future eruptions. Oceanography,
413	31(1), 114–123. https://doi.org/10.5670/oceanog.2018.117
414	Wilcock, W., Tolstoy, M., Waldhauser, F., Garcia, C., Tan, Y. J., Bohnenstiehl, D. R., et al.
415	(2016). The 2015 eruption of Axial Seamount: Seismic constraints on caldera dynamics.
416	Science, 354(6318), 1395–1399. https://doi.org/10.1126/science.aah5563
417	Wilson, D. S. (1988). Tectonic history of the Juan de Fuca Ridge over the last 40 million years.
418	J. Geophys. Res., 93(B10), 11863-11876.
419	Xu, M. and M.A. Tivey, (2016). Investigation of a marine magnetic polarity reversal boundary in
420	cross-section at the northern boundary of the Kane Megamullion, Mid-Atlantic Ridge
421	23°40'N, Jour. Geophys. Res., 121, 3161-3176, doi: 10.1002/2016JB012928.
422	

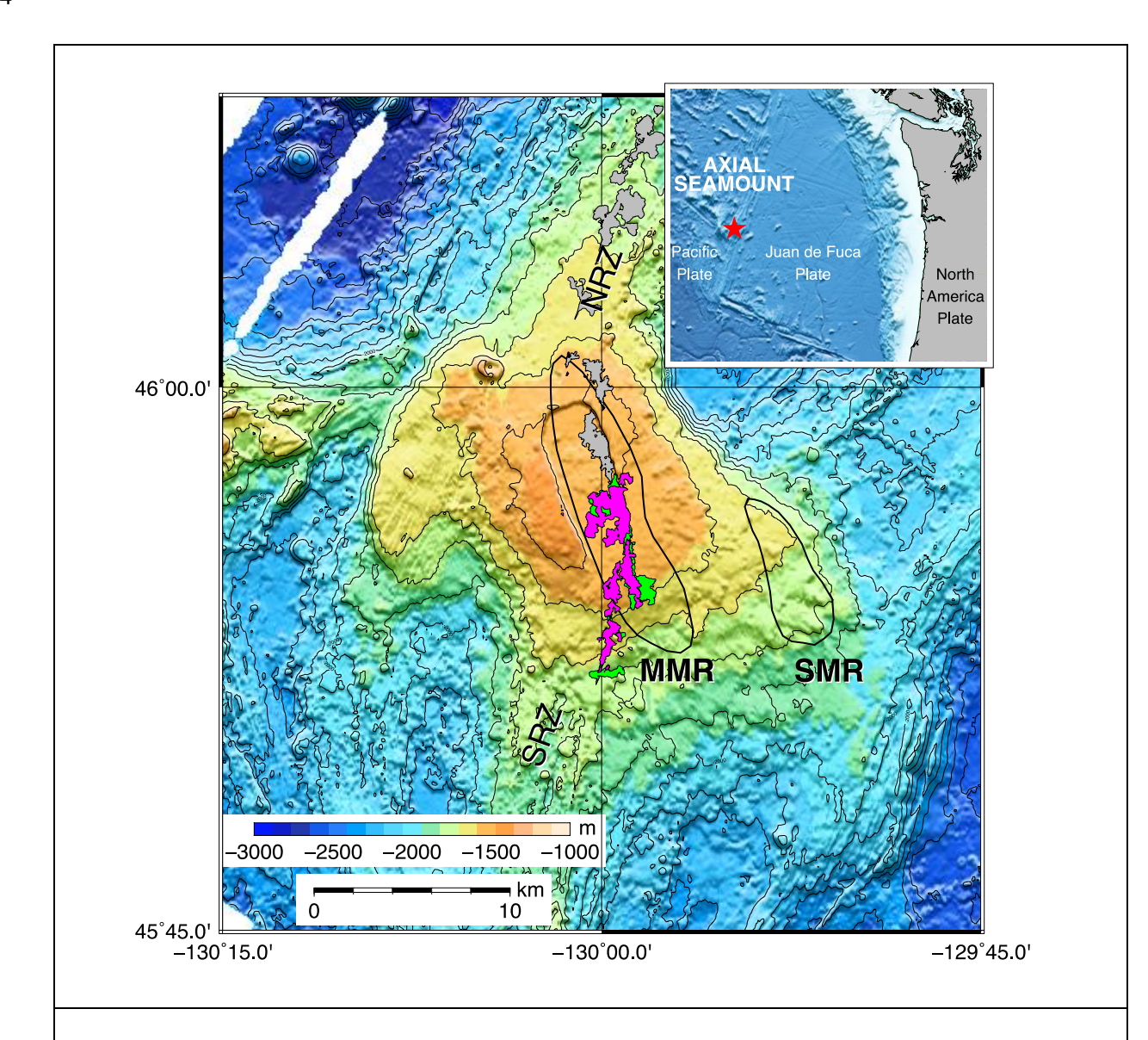


**Figure 1.** Bathymetry map of Axial Seamount showing the location of the caldera, magma bodies (main magma reservoir (MMR), secondary magma reservoir (SMR)), and lava flows with an inset map showing tectonic context (Adapted from Arnulf et al., 2018 and Waldhauser et al., 2020). Gray shaded areas are 2015 flows, magenta areas are 2011 flows and green areas are 1998 flows (largely buried by 2011 lava). NRZ is North Rift Zone and SRZ is South Rift Zone.

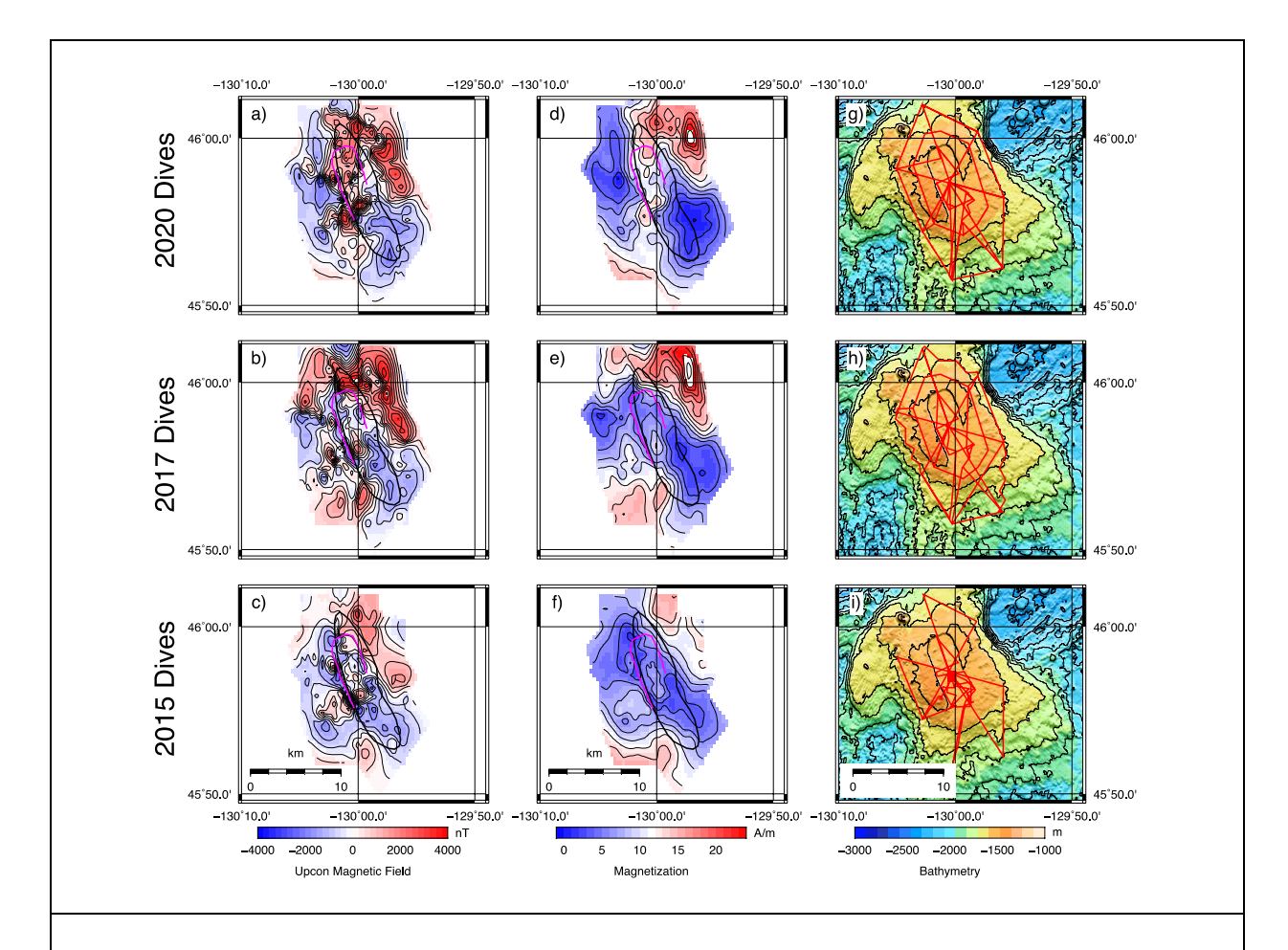


**Figure 2.** Processed magnetic results of AUV Sentry dives gathered over Axial Seamount in 2015, 2017, and 2020 with the caldera region (purple line) and MMR (bold black line) indicated. a), b), c) Sentry magnetic field (cont. level 500 nT). d), e), f) Crustal magnetization, cont. level 2 A/m). g), h), i) Repeat Sentry tracklines (red) over bathymetry map (Cont. level 100 m), excluding some lines that were only in the 2020 survey.

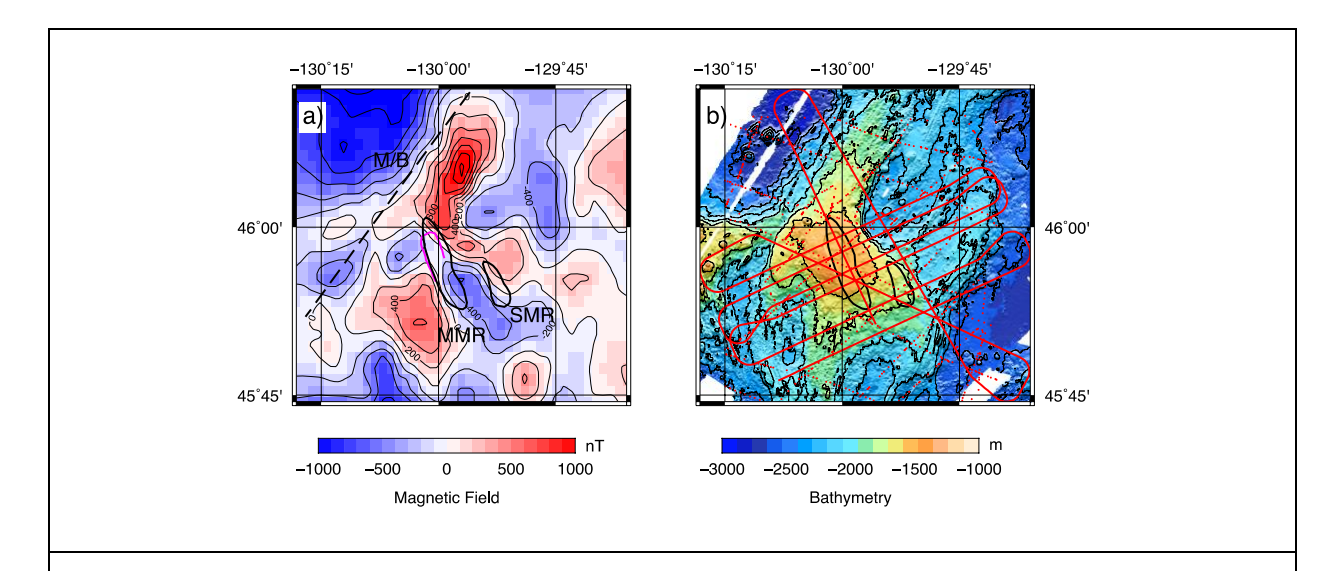


**Figure 3.** a) Reduced-to-the-pole sea surface magnetic anomaly over Axial Seamount from a compilation of 2019 magnetic data (MGL2019) and older existing sea surface coverage from the NCEI database. Contour interval is 200 nT. Black lines indicate outlines of MMR (west) and SMR (east) and purple line is outline of the caldera as noted in Figure 1. Black dashed line indicates the western edge of normal polarity Brunhes chron and beginning of the reversed Matuyama chron (M/B). b) Multibeam bathymetry of the Axial Seamount, contour interval is 200 m. Red lines indicate sea surface magnetic data coverage.

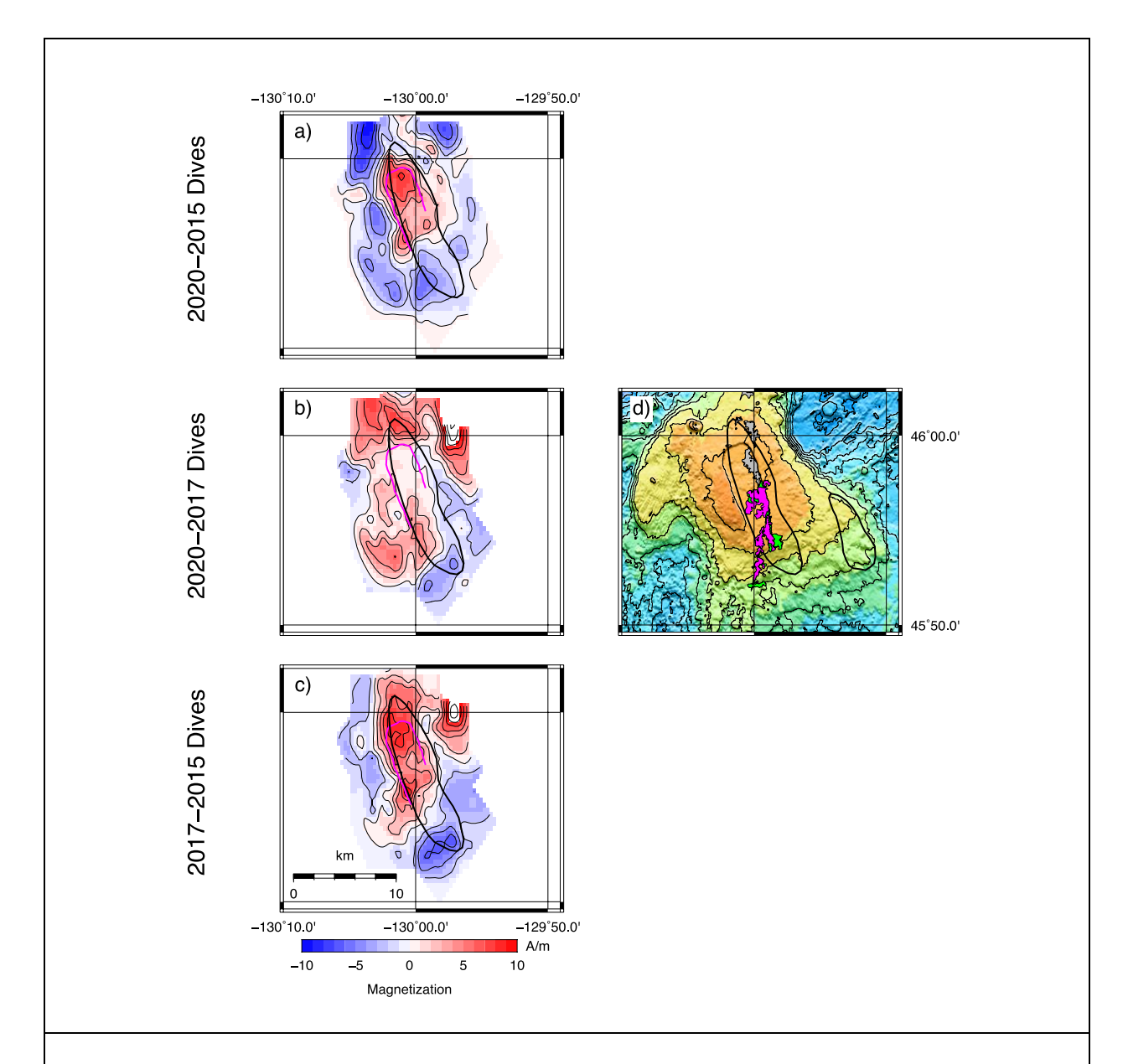
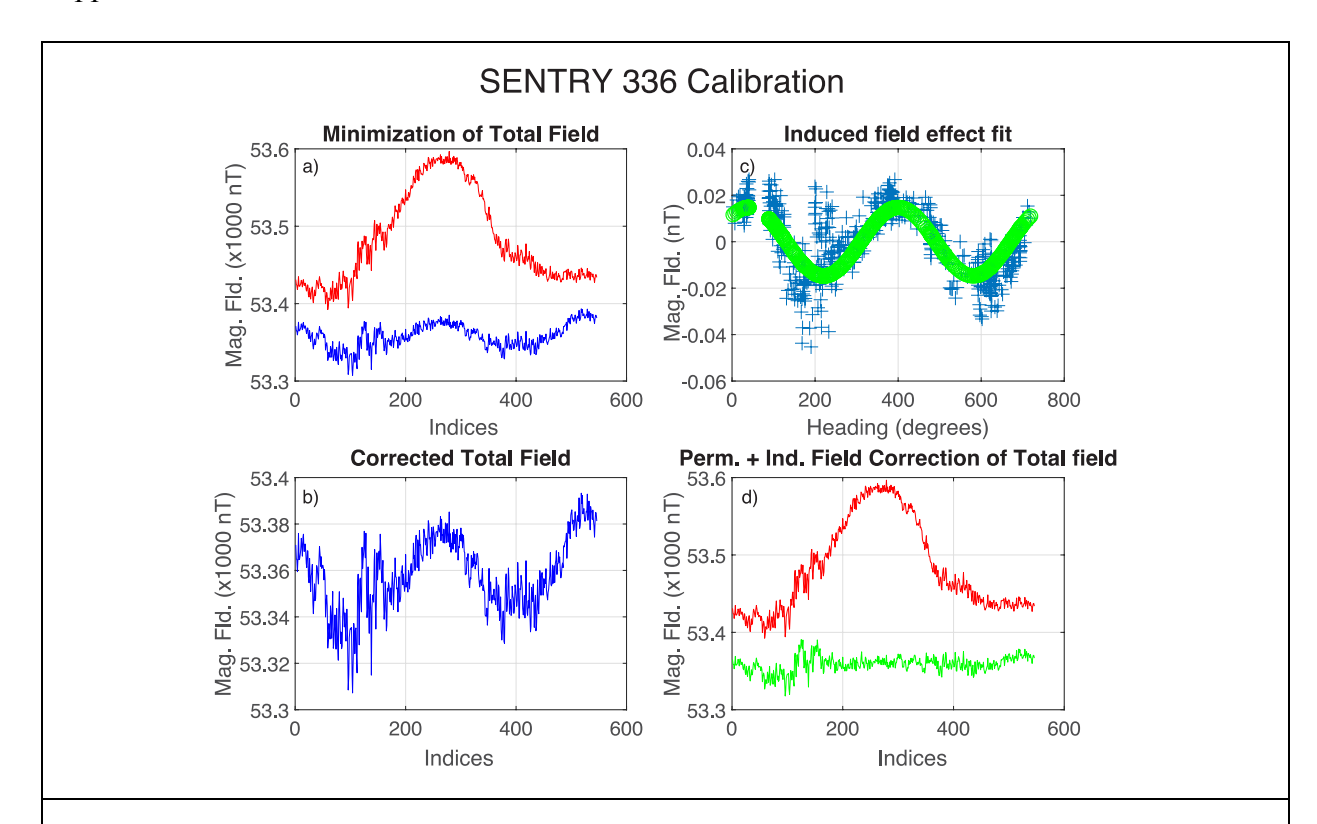
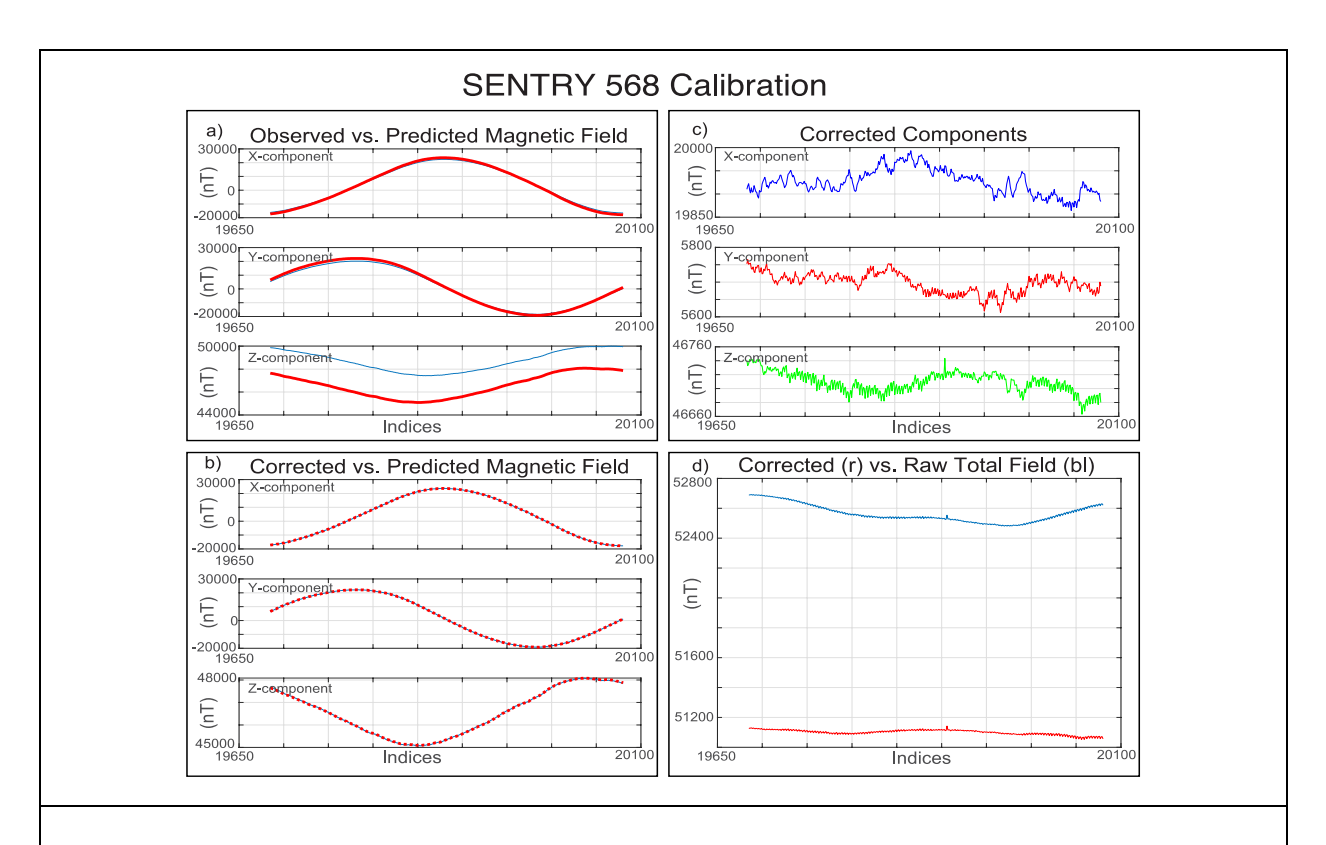


**Figure 4.** Differences in inversion results between different years (a) 2020 - 2015, (b) 2020 - 2017, and (c) 2017 - 2015 highlighting the increase in magnetization within the caldera over time. Contour interval is 2 A/m. Caldera region (purple) and MMR (black) indicated. d) Bathymetry with lava flow eruptions color coded by year: green (1998), magenta (2011), gray (2015). Bold black lines indicate the subcrustal magma anomalies MMR and SMR regions as noted in Figure 1.

## Supplemental Material



**Supplemental Figure S1.** Example of compass-swing calibration summary for calibration spins of Sentry Dive 336 showing **a)** observed total field (red) and total field corrected for permanent field effect (blue) **b)** field corrected for permanent field effect **c)** fit for induced field component (green) vs. observed data (blue) and **d)** final corrected field (green) compared with observed uncorrected field (red). Final variation level was 72 nT.



**Supplemental Figure S2.** Example of vector calibration summary for calibration spins of Dive 568 showing **a)** observed magnetic field (blue) and predicted magnetic field (red) using information about the vehicle's attitude and the IGRF value for the given location, **b)** corrected (blue) and predicted (red) magnetic field, **c)** corrected components of the magnetic field, and **d)** total corrected field (red) compared to raw field (blue). Final variation level was 89 nT.

Supplemental Table 1. Summary of calibration results for Sentry Dives showing original total field variation versus the final corrected total field variation.

Dive Number	Original Total Field Variation	Corrected Total Field Variation
	(nT)	(nT)
336	204	72
337	362	88
338	247	42
339	268	73

455

340	488	50
341	354	32
442	118	27
443	561	77
444	135	67
445	105	38
446	221	36
562	275	120
563	151	44
564	143	46
565	109	44
566	101	55
567	143	60
568	211	89
Average	233 ± 134	59 ± 24